

1 **A simple self-adjusting model for correcting the blooming effects in DMSP-**
2 **OLS nighttime lights images**

3
4 Xin Cao¹, Yang Hu¹, Xiaolin Zhu^{2*}, Feng Shi³, Li Zhuo⁴, Jin Chen¹

5
6 1. State Key Laboratory of Earth Surface Processes and Resource Ecology, Faculty of
7 Geographical Science, Beijing Normal University, Beijing 100875, China

8 2. Department of Land Surveying and Geo-Informatics, The Hong Kong Polytechnic University,
9 Hong Kong, China

10 3. Institute of Science and Technology for Development of Shandong, Qilu University of
11 Technology (Shandong Academy of Science), Jinan 250014, China

12 4. Guangdong Provincial Key Laboratory of Urbanization and Geo-simulation & Center of
13 Integrated Geographic Information Analysis, School of Geography and Planning, Sun Yat-sen
14 University, Guangzhou, Guangdong 510275, China

15
16 *Corresponding author:

17 Xiaolin Zhu

18 Address: The Hong Kong Polytechnic University, Room ZS621, South Wing, Block Z, 181
19 Chatham Road South, Kowloon, Hong Kong.

20 Phone: 852-2766-5976; Email: xiaolin.zhu@polyu.edu.hk

21 **Abstract**

22 Night-time light (NTL) data from the Defense Meteorological Satellite Program (DMSP)
23 Operation Linescan System (OLS) provide important observations of human activities; however,
24 DMSP-OLS NTL data suffer from problems such as saturation and blooming. This research
25 developed a self-adjusting model (SEAM) to correct blooming effects in DMSP-OLS NTL data
26 based on a spatial response function and without using any ancillary data. By assuming that the
27 pixels adjacent to the background contain no lights (i.e., pseudo light pixels, PLPs), the blooming
28 effect intensity, a parameter in the SEAM model, can be estimated by pixel-based regression
29 using PLPs and their neighboring light sources. SEAM was applied to all of China, and its
30 performance was assessed for twelve cities with different population sizes. The results show that
31 SEAM can largely reduce the blooming effect in the original DMSP-OLS dataset and enhance its
32 quality. The images after blooming effect correction have higher spatial similarity with Suomi
33 National Polar-orbiting Partnership Visible Infrared Imaging Radiometer Suite (VIIRS) images
34 and higher spatial variability than the original DMSP-OLS data. We also found that the average
35 effective blooming distance is approximately 3.5 km in China, which may be amplified if the
36 city is surrounded by water surfaces, and that the blooming effect intensity is positively
37 correlated to atmospheric quality. The effectiveness of the proposed model will improve the
38 capacity of DMSP-OLS images for mapping the urban extent and modeling socioeconomic
39 parameters.

40

41 **Keywords:**

42 DMSP-OLS, nighttime light, blooming, spatial response function, self-adjusting model

43 **1. Introduction**

44 Night-time light (NTL) data records nocturnal artificial light on the Earth's surface and
45 provides unique observations for human activities (Elvidge et al., 1997a; Elvidge et al., 2001).
46 Two main datasets that offer global coverage are available for NTL information, the digital
47 archive of annual composite images since 1992 from the Operational Linescan System (OLS)
48 instrument onboard Defense Meteorological Satellite Program (DMSP) satellite and nighttime
49 light images from the Visible Infrared Imaging Radiometer Suite (VIIRS) instrument onboard
50 the Suomi National Polar-orbiting Partnership (Suomi-NPP) satellite launched in 2011 (Bennett
51 and Smith, 2017; Elvidge et al., 2017). In recent decades, NTL data have been widely used in
52 socioeconomic and environmental research, including urbanization delineation and spatial
53 distribution analyses (Small et al., 2005; Cao et al., 2009; Zhou et al., 2014; Letu et al., 2015;
54 Xie and Weng, 2017), economic development or decline monitoring (Elvidge et al., 1997a;
55 Henderson et al., 2012; Rohner et al., 2013), population density mapping (Zhuo et al., 2009;
56 Townsend and Bruce, 2010), electricity consumption modeling (Lo, 2002; Letu et al., 2010;
57 Townsend and Bruce, 2010; Cao et al., 2014; Proville et al., 2017), environmental issues such as
58 light pollution (Cinzano et al., 2001; Longcore and Rich, 2004; Butt, 2012; Rodrigues et al., 2012;
59 Falchi et al., 2016), air quality (Wang et al., 2016) and CO₂ emissions (Zhang et al., 2017;
60 Proville et al., 2017).

61 DMSP-OLS provides the longest observations of NTL information, from 1992 to 2013, an
62 unparalleled dataset for studying historical artificial lights; however, it suffers from four main
63 problems: coarse spatial resolution, lack of onboard calibration, saturation and blooming (Imhoff
64 et al., 1997; Small et al., 2011; Small et al., 2005; Elvidge et al., 2007; Bennett and Smith, 2017).
65 The spatial resolution of DMSP-OLS data is 2.7 km, whereas NPP-VIIRS offers a finer

66 resolution of 742 m (Bennett and Smith, 2017). DMSP-OLS NTL annual composite data
67 available from 1992 to 2013 were acquired by sensors onboard six different satellites without
68 onboard calibration mechanisms (Elvidge et al., 2009). Pandey et al. (2017) summarized several
69 algorithms for the relative calibration of DMSP NTL data based on the concept of pseudo-
70 invariant features (PIFs) and found that global-scale calibration methods outperform regionally
71 based calibration methods. The saturation problem resulted from the small (6-bit) quantization
72 and low dynamic range of OLS data, which led to the inability of the OLS to record light
73 brighter than a digital number (DN) value of 63 (Elvidge et al., 1997b). Combined with
74 information about vegetation indices, land surface temperature (LST) or socioeconomic statistics,
75 researchers have developed several methods to effectively mitigate the saturation of OLS data
76 (Lu et al., 2008; Zhang et al., 2013; Zhuo et al., 2015; Hao et al., 2015; Cao et al., 2014). The
77 blooming effect, or overglow, refers to the lighted areas detected by the OLS larger than the
78 geographic extents of the light sources, which leads to the overestimation of the extent of urban
79 areas (Small and Elvidge, 2013). The blooming effect is more serious for coarser nighttime light
80 images (Kyba et al., 2014). For example, the blooming effect was also observed in monthly
81 VIIRS composite data (Levin, 2017) but was not as serious as in DMSP-OLS data. The
82 blooming effect brings difficulties, bias, and challenges to the applications of nighttime light data.
83 However, only a few studies have quantitatively evaluated the blooming effect (Small et al.,
84 2005; Townsend and Bruce, 2010; Hao et al., 2015), and no consensus on blooming effect
85 correction has yet been reached (Bennett and Smith, 2017).

86 The possible reasons for the blooming effect include the large footprints of the OLS sensor
87 (Elvidge et al., 2004; Elvidge et al., 2013), the scattering of light in the atmosphere, and the
88 accumulation of geo-location errors in the compositing process (Richter, 1996; Small et al., 2005;

89 [Small and Elvidge, 2013](#); [Kyba et al, 2014](#)). Existing studies have also found that the blooming
90 effect is related to the equivalent diameter for contiguous lighted areas ([Small et al., 2005](#)), light
91 source strength ([Townsend and Bruce, 2010](#)), adjacent water or snow surfaces ([Bennett and
92 Smith, 2017](#)), and thin clouds ([Letu et al., 2015](#)). To reduce the blooming effect in urban area
93 detection, [Zhou et al. \(2014\)](#) used a water mask to exclude pixels with water percentages over 50%
94 along shorelines. Some saturation correction methods, such as the Vegetation Adjusted NTL
95 Urban Index (VANUI) ([Zhang et al., 2013](#)) and the Vegetation Temperature Light Index (VTLI)
96 ([Hao et al., 2015](#)), can also alleviate the blooming effect. However, since their main purposes are
97 limited, their effectiveness and flexibility to tackle the blooming effect with inadequate
98 validations is not clear. [Small et al. \(2005\)](#) suggested employing a scale-dependent blooming
99 correction procedure after finding a linear relationship between lit area and blooming distance
100 for 10 illuminated islands as samples. However, the method's effectiveness over non-coastal
101 areas has not yet been verified. [Townsend and Bruce \(2010\)](#) developed the Overflow Removal
102 Model (ORM), which corrects the blooming effect by using the relationship between regional
103 light intensity and blooming distance considering the effects of annual atmospheric conditions,
104 topography and elevation. However, the method needs auxiliary data, which may not always be
105 available for locations in developing countries where NTL imagery may provide the most insight
106 regarding economic development. [Li et al. \(2017\)](#) simulated the DMSP-OLS composites from
107 the NPP-VIIRS images by using a power function and a Gaussian low-pass filter. This method
108 can reduce the blooming effect in the simulated DMSP-OLS images because the NPP-VIIRS
109 images have little blooming effect ([Bennett and Smith, 2017](#)). However, this method is not able
110 to correct the DMSP-OLS images before 2012, when NPP-VIIRS images became available.
111 Recently, [Abrahams et al \(2018\)](#) deblurred the DMSP images based on the assumption that light

112 was blurred via a symmetric Gaussian point-spread function (PSF); the dimension of the PSF
113 could be calibrated by the frequency of illumination. This new deblurring method is effective in
114 improving DMSP annual composite images. However, it is limited in processing annual
115 composite images because it needs an auxiliary dataset that records the frequencies of
116 illumination of each pixel, which may be less accurate in cloudy regions such as tropical
117 countries.

118 To this end, we developed the self-adjusting model (SEAM) based on a spatial response
119 function (SRF) to correct the blooming effect without using other ancillary data. We tested the
120 SEAM model to correct the blooming effect in China and evaluated the effectiveness of the
121 SEAM model in twelve cities with various population scales by comparison with NPP-VIIRS
122 data, the VANUI and VTLI methods, as well as the accuracy of urban area extraction. This
123 simple blooming effect correction model is expected to be used as a preprocessing method for
124 the DMSP-OLS NTL data.

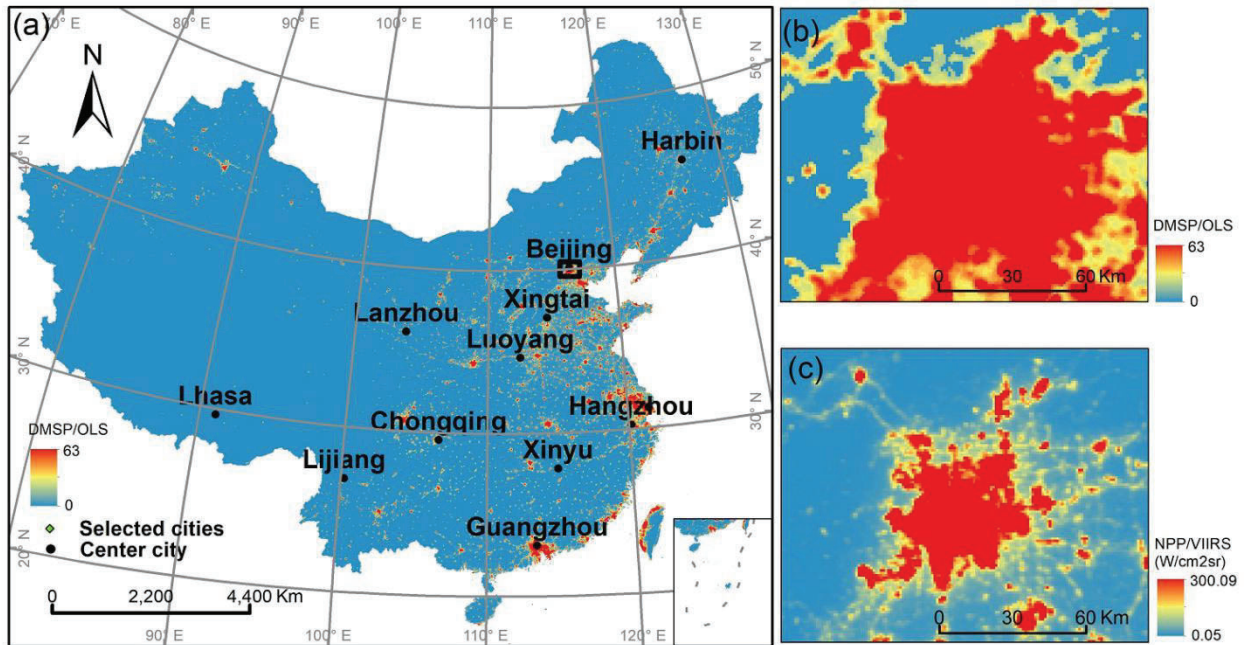
125

126 **2. Data and methods**

127 **2.1 Study area and data**

128 We used DMSP-OLS stable NTL data for China in 2013 (Fig. 1a) to test the blooming
129 correction method proposed by this study. Twelve cities with different size of population and
130 levels of economic development were selected to visually and quantitatively evaluate the
131 performance of the blooming effect correction model. These cities are categorized into six
132 groups by population: >10 million (Shanghai and Beijing), 5–10 million (Chongqing and
133 Guangzhou), 3–5 million (Harbin and Hangzhou), 1–3 million (Lanzhou and Luoyang), 0.5–1
134 million (Xinyu and Xingtai), and <0.5 million (Lhasa and Lijiang). The twelve center cities are

135 marked by black points in Fig. 1(a). Fig. 1 (b) shows an enlarged sub-region of the DMSP-OLS
136 image covering Beijing. Because ground truth values of light intensity are not available, the
137 NPP-VIIRS nighttime light images in 2013 are used as a reference to evaluate the effectiveness
138 of the proposed model, assuming the blooming effects in the NPP-VIIRS images are sufficiently
139 weak (Li and Zhou, 2017) (Fig. 1c). The DMSP-OLS and NPP-VIIRS nighttime light data
140 (hereafter DMSP and VIIRS for short) were downloaded from the National Oceanic and
141 Atmospheric Administration (NOAA) National Centers for Environmental Information
142 (<http://ngdc.noaa.gov/eog/download.html>). The DMSP image downloaded was
143 “F182013.v4c_web.stable_lights.avg_vis.tif”. By geolocation processing, the stable lights were
144 summarized to grids with a nominal resolution of 30 arc seconds, which equals 1 km at the
145 equator. For convenience, this study used “pixel” to represent the “grid” of the DMSP stable
146 NTL data. Four seasonal VIIRS datasets were downloaded in 2013, and we used the average of
147 the four seasonal VIIRS images as the yearly VIIRS image in 2013 to match the DMSP image.
148 All images were re-projected to the same coordinate system, WGS_1984_UTM49N. Then, the
149 VIIRS data were resampled to the resolution of DMSP images and co-registered to the DMSP
150 images using 20 GCPs selected from isolated cities without saturated pixels (see details in
151 Supplementary Data).



152

153 Fig. 1. The DMSP-OLS image of China in 2013 (a). Right column shows the enlarged DMSP-
 154 OLS image (b) and NPP-VIIRS image (c) for Beijing (black box in a). The green points with
 155 serial numbers are the 20 cities selected to investigate the effective blooming distance (see Table
 156 3). The black points indicate the 12 cities used for evaluation.

157

158 To assess the performance of the proposed blooming effect removal model, we used Moderate
 159 Resolution Imaging Spectroradiometer (MODIS) Normalized Difference Vegetation Index
 160 (NDVI) and Land Surface Temperature (LST) products to implement two existing DMSP
 161 correction models: VANUI (Zhang et al., 2013) and VTLI (Hao et al., 2015). The MODIS
 162 monthly composite of NDVI and nighttime LST data for 2013 were selected for this study. The
 163 results from the proposed method were compared with these two existing methods. We also
 164 compared urban extent extracted from the blooming-adjusted results with a reference urban
 165 extent map, the Global Urban Footprint (GUF) map (Esch et al., 2017). The GUF data are
 166 provided by the German Aerospace Center (DLR, <https://www.dlr.de/>) with a spatial resolution
 167 of 2.8 arc seconds (approximately 75 m in mid-latitudes). This dataset was generated using data

168 collected by the TerraSAR-X/TanDEM-X satellites between 2011 and 2012, which matches the
169 time of the NTL data in this study.

170 The other data used to aid this research included the ground-level PM2.5 data in 2013 (van
171 Donkelaar et al., 2016) (<http://fizz.phys.dal.ca/~atmos/martin/>). This dataset is satellite-derived
172 and adjusted by geographically weighted regression with a 0.01° grid. We also used the
173 GlobeLand30-2010 product (Chen et al., 2015; Chen et al., 2016) (<http://www.globeland30.org>)
174 to provide further land cover information such as water and urban area.

175

176 **2.2. Self-adjusting blooming effect correction model**

177 *(1) Theoretical basis*

178 Theoretically, the blooming effects on individual pixels in DMSP images can be described
179 by the sensor spatial response function (SRF), which is usually modeled as kernel functions, such
180 as the Gaussian function and inverse distance function (Liang, 2003). In this study, the inverse
181 distance function is used to approximate the SRF considering that light intensity attenuates with
182 squared distance:

$$183 \quad SRF = f(d) = \frac{a}{d^2} \quad (1)$$

184 where d is the spatial distance corresponding to the sensor ground instantaneous field of view
185 (IFOV) and a is a coefficient. In a satellite image, the SRF implies the degree of signals beyond
186 the pixel size that contribute to the pixel value, i.e., a target pixel value contains the contributions
187 of its neighboring pixels. Therefore, the observed value of a target pixel (R) can be written as:

$$188 \quad R = \beta \times R_0 + \left(\sum_{i=1}^N f(d_i) \times R_i + b \right) \quad (2)$$

189 The first term on the right side of Eq. (2) indicates the light signal from the target pixel, and the
190 second term is the incoming light from neighboring pixels via the SRF. R_0 is the actual light
191 emitted by the target pixel, β is a coefficient representing the percentage of remaining light after
192 deducting out-scattering of R_0 , R_i is the pixel value of the i -th neighboring pixel selected from a
193 moving window, N is the total number of neighboring pixels, and b is the background value. The
194 pixel value R_i of the i -th neighboring pixel includes its actual light and the blooming light it
195 received; R_i in Eq. (2) thus allows the model to count both the direct blooming effect (from
196 neighbors to the target) and the indirect blooming effect (from other pixels to neighbors and then
197 to the target). In this study we assumed that out-scattering is linearly related to the intensity of
198 the light source, i.e., β is a constant value. We also assumed that neighboring pixels that are
199 brighter than the target pixel (i.e., $R_i > R$) make a net blooming contribution because the out-
200 scattering of the target pixel can offset the contribution from darker neighboring pixels.
201 Therefore, the key to remove the blooming effect is to model the ambient incoming light, i.e., to
202 estimate the SRF in Eq. (2). For a given DMSP pixel, the R and R_i of its neighbors are known but
203 not R_0 . To make Eq. (2) solvable, we need to search some pixels in the DMSP image that have R_0
204 equal to zero, i.e., these pixels do not have any artificial light source and are only lit by neighbors
205 due to the blooming effect. We defined these pixels as ‘pseudo light pixels’ (PLPs), for which
206 the DN values (R') entirely come from the neighboring light pixels:

$$207 \quad R' = \sum_{i=1}^N f(d_i) \times R_i + b \quad (3)$$

208 Taking Eq. (1) into Eq. (3), we obtain:

$$209 \quad R' = a \times \sum_{i=1}^N \frac{R_i}{d_i^2} + b \quad (4)$$

210 In Eq. (4), the unknown coefficients a and b can be estimated by regression analysis using
211 the PLPs and their neighboring light pixels.

212 ***(2) Self-adjusting model implementation steps***

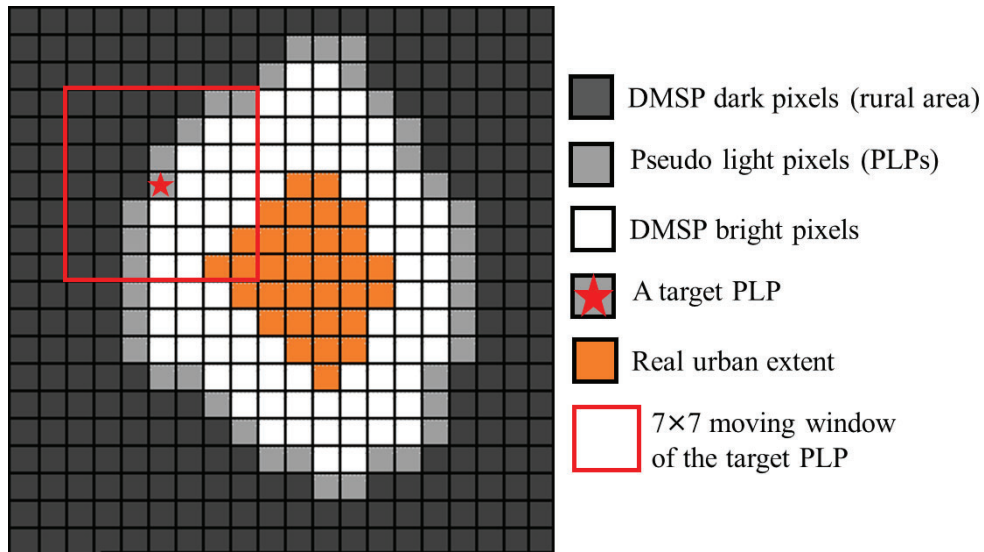
213 *Step 1: Search for pseudo light pixels*

214 Based on the above concept, this first step is to find the PLPs in a DMSP image to estimate
215 the coefficients a and b . As the diagram shows in Fig. 2, the intensity of artificial lights in DMSP
216 images generally decreases from a city center to its edges (Zhou et al., 2015), with the brightest
217 pixels (DN = 63) located in the city centers and the darkest pixels (DN = 0) close to rural areas
218 (background areas). We thus assume that PLPs can be selected from pixels next to the urban
219 edges, i.e., the pixel itself shows weak brightness (pixel value > 0) but one or more of its eight
220 neighbors are dark (pixel value = 0) in the DMSP/OLS images (e.g., the light gray pixels in Fig.
221 2). As a result, the DN values of these pixels should mainly come from their neighboring pixels
222 due to the blooming effect. These pixels are selected as the PLPs and their pixel values can be
223 described by Eq. (4).

224 *Step 2: Select effective neighboring pixels for PLPs*

225 For each PLP, we need to select its effective neighboring pixels, i.e., the pixels within the
226 effective blooming distance, for calculating its value by Eq. (4). By visual comparison between
227 DMSP image and a referenced urban extent derived from a global 30-m land cover map (Chen et
228 al., 2015) for 20 isolated cities in China with relatively regular shape (Fig. 1a, marked by green
229 points and labeled by numbers), the urban extent from GlobeLand30 was used as a reference to
230 measure the blooming effect distance of DMSP data. For each PLP of a city, we can search a
231 nearest distance to the urban region of GlobeLand30, and the average distance of all the PLPs to
232 their nearest urban region represent the effective blooming distance of the city. The effective

233 blooming distance ranges from 2.22 to 4.38 km (see Table 3 in Discussion Session for details),
 234 and the average value is 3.53 km, which is equivalent to 3.5 pixels in DMSP images. Based on
 235 Eq. (1), the neighboring pixels beyond 3.5 km should have very weak influence on PLPs.
 236 Therefore, a 7×7 moving window (with a PLP as the center) was suggested to search the
 237 effective neighboring pixels (Fig. 2). For each PLP, only the pixels within the 7×7 window with
 238 DN values larger than that of the PLP are chosen as effective neighboring pixels to compute the
 239 weighted sum in Eq. (4). The spatial distance between the PLP and its neighboring pixels is
 240 calculated as the Euclidean distance between the centers of the pixels.



241
 242
 243 Fig. 2. Diagram of selecting pseudo light pixels (PLPs) and their effective neighboring pixels
 244 within a 7×7 moving window
 245

246 *Step 3: Remove blooming effect for each bright DMSP pixel*

247 For each bright DMSP pixel with DN larger than 0 (named as the target pixel), we can
 248 apply Eq. (2) to estimate the light intensity excluding the blooming effect if we know the
 249 coefficients a and b . In one DMSP image, we can select enough PLPs and their effective
 250 neighboring pixels following step 1 and 2 and then estimate a and b by linear regression.
 251 However, the estimated a and b are global parameters for the entire DMSP image, which may

252 not be optimal values for removing the blooming effect for all individual DMSP pixels.
 253 Considering that the intensity of the blooming effect might be affected by some local factors,
 254 such as the total light intensity of surrounding urban pixels (Townsend and Bruce, 2010), local
 255 atmospheric conditions (Small and Elvidge, 2013) and adjacent water bodies or snow (Bennett
 256 and Smith, 2017), the coefficients in Eq. (4) may change pixel-by-pixel, and local PLPs were
 257 thus selected to estimate the coefficients for each target pixel. Specifically, for each DMSP pixel
 258 with DN larger than 0, PLPs were selected within a radius range of 150 km; a 150-km radius was
 259 used because (1) enough PLPs can be selected and (2) atmospheric conditions (e.g., particulate
 260 matter concentrations, PM_{2.5} and PM₁₀) within this range are relatively uniform (Hu et al., 2014).
 261 For each PLP, its effective neighboring pixels were selected within the 7×7 window following
 262 step 2. Then, the values of PLPs and the weighted sum of their effective neighboring pixels were
 263 used as dependent and independent variables to estimate parameters a and b in Eq. (4) by
 264 ordinary least squares linear regression. Finally, for the target DMSP pixel, its pixel value
 265 without blooming effects (R^*) can be estimated by:

$$R^* = R - \left(\hat{a} \times \sum_{i=1}^N \frac{R_i}{d_i^2} + \hat{b} \right) \quad (5)$$

267 where R^* is the first term on the right side of Eq. (2), $\beta \times R_0$, the real artificial light after deducting
 268 out-scattering. \hat{a} and \hat{b} are estimated coefficients. R_i is the DN value of the effective
 269 neighboring pixels of the target pixel and $R_i > R$. Extremely large difference between adjacent
 270 pixels may exist in the original DMSP image. This extreme large difference will lead to
 271 unreliable results (e.g., negative brightness values) of blooming adjustment using Eq. (5). To
 272 mitigate the impact of this extreme situation, we then introduced a mean filter by using a 3×3

273 moving window to reduce the extremely large differences among adjacent pixels while
274 maintaining the spatial pattern of the original DMSP image.

275 **2.3 Performance assessment of blooming effect removal**

276 To evaluate the performance of SEAM for blooming effect removal, we compared SEAM
277 with two other vegetation adjusted methods, VANUI (Eq. 6) and VTLI (Eq. 7), to correct the
278 DMSP data. VANUI combines the MODIS NDVI with the NTL data based on the hypothesis
279 that the vegetation abundance is highly negatively correlated with the distribution of impervious
280 surfaces (Zhang et al., 2013). VTLI incorporates the land surface temperature (LST) information
281 with the vegetation index due to the temperature being higher in the center of the city (Hao et al.,
282 2015). The monthly maximum composite of NDVI and nighttime LST for MODIS in 2013 was
283 used to calculate VANUI and VTLI, respectively:

$$284 \quad \text{VANUI} = (1 - \text{NDVI}) \times \text{NTL} \quad (6)$$

$$285 \quad \text{VTLI} = (1 - \text{NDVI}) \times \text{LST} \times \text{NTL} \quad (7)$$

286 In summary, for the original DMSP image, three blooming-adjusted results were obtained
287 by the proposed SEAM model (hereafter DMSP-BC) and the VANUI and VTLI methods,
288 respectively. Two evaluation indicators, the correlation coefficient between the evaluated image
289 and the reference image (i.e., VIIRS image) and the spatial variability of the evaluated image,
290 were used to assess the effectiveness of different models for blooming effect removal.

291 *1) Correlation coefficients (R) between VIIRS images and the evaluated images.* R is used
292 to measure the correlation between VIIRS image and DMSP, DMSP-BC, VANUI and VTLI
293 images. The SEAM model cannot remove the saturation effect, and pixels with DN values of 63
294 in the DMSP images and corresponding areas in the VIIRS images were thus excluded when
295 calculating the correlation coefficients. If blooming effect correction is effective, the blooming-

296 adjusted images are expected to have higher R values with the VIIRS image than with the
297 original DMSP image. The correlation coefficients were computed for each city using pixels
298 within the minimum bounding rectangle of the city extent detected from the VIIRS image.

299 2) *Spatial variability of pixel values within urban areas of each nighttime image.*
300 Theoretically, the blooming effect makes DMSP images ‘smooth’ and decreases the spatial
301 variability of pixel values in urban regions compared with the corresponding VIIRS images,
302 which have minimal blooming effects. After correcting the blooming effect with the SEAM
303 method, the spatial variability of DMSP-BC is expected to be higher than that of the original
304 DMSP image. Since the DN values of DMSP images and VIIRS images are not comparable in
305 value, we used the coefficient of variation (CV) to measure the relative spatial variability:

$$306 \qquad CV = std(R) / mean(R) \qquad (8)$$

307 where R is the DN value in each city and $std(R)$ and $mean(R)$ are the standard deviation and
308 mean of the DN values, respectively. CV was calculated for VIIRS, DMSP, DMSP-BC, VANUI
309 and VTLI images.

310 We also evaluated the performance of NTL data for urban area extraction by comparing the
311 results from DMSP and DMSP-BC with Global Urban Footprint (GUF) data as reference data.
312 Because GUF data have higher spatial resolution (approximately 75 m in mid-latitudes), we first
313 aggregated the data to 1-km spatial resolution (GUF-1km) to match the DMSP data. Then, we
314 adopted the local optimized threshold method (Cao et al., 2009) to extract urban areas from
315 DMSP and DMSP-BC images. The local optimized threshold is the one among all tested
316 thresholds that can obtain the highest Kappa coefficient of the extracted urban areas using GUF-
317 1km as reference data.

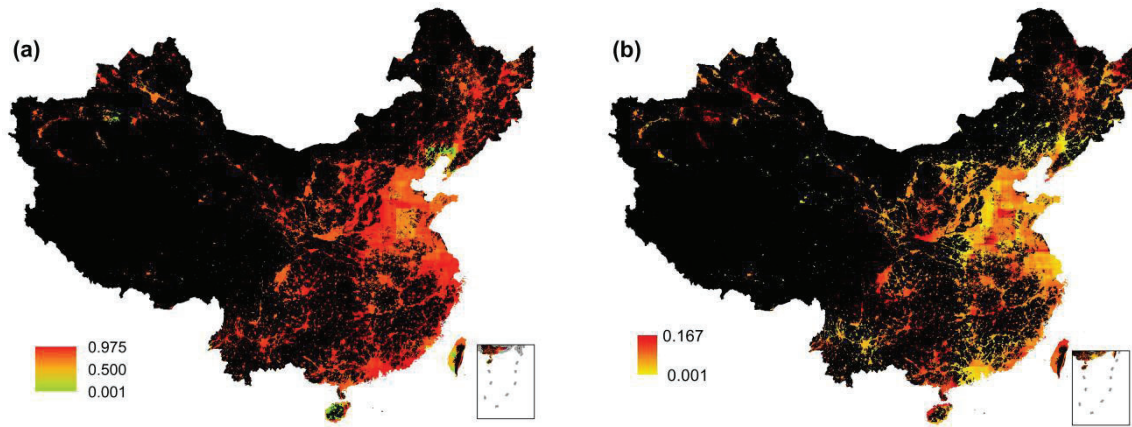
318

319 **3. Results**

320 **3.1 Parameter estimation in the SEAM model**

321 As explained in section 2.2, for each pixel with DN values larger than 0 in the DMSP image
322 of China, a local regression model was built to estimate parameters a and b using PLPs selected
323 in a neighborhood. Fig. 3 shows the spatial distribution of the pixel-based regression results. The
324 coefficients of determination (R^2) for the pixel-based regression models are plotted in Fig. 3 (a).
325 Over 97% of the pixels achieve a high coefficient of determination (>0.7), whereas some pixels
326 in coastal areas and inland northwest areas have lower coefficients of determination. The
327 regression models for pixels with coefficients of determination less than 0.7 were replaced by
328 those with the highest coefficients of determination close to these pixels. Fig. 3 (b) indicates the
329 spatial distribution of regression coefficient a in Eq. (4), which represents the intensity of the
330 blooming effect. A higher regression coefficient a indicates a stronger blooming effect and more
331 lights scattered from a pixel to its neighborhood. We found that the regression coefficient a is
332 positively correlated with annual mean $PM_{2.5}$ concentrations ($R^2 = 0.3223$, $p < 0.0001$) for all of
333 China, excluding the pixels with $DN=0$. This result suggests that the intensity of the blooming
334 effect may be influenced by atmospheric conditions.

335



336

337 Fig. 3 Regression results for pixel-based regression models; (a) coefficients of determination
 338 (R^2), and (b) regression coefficient a .

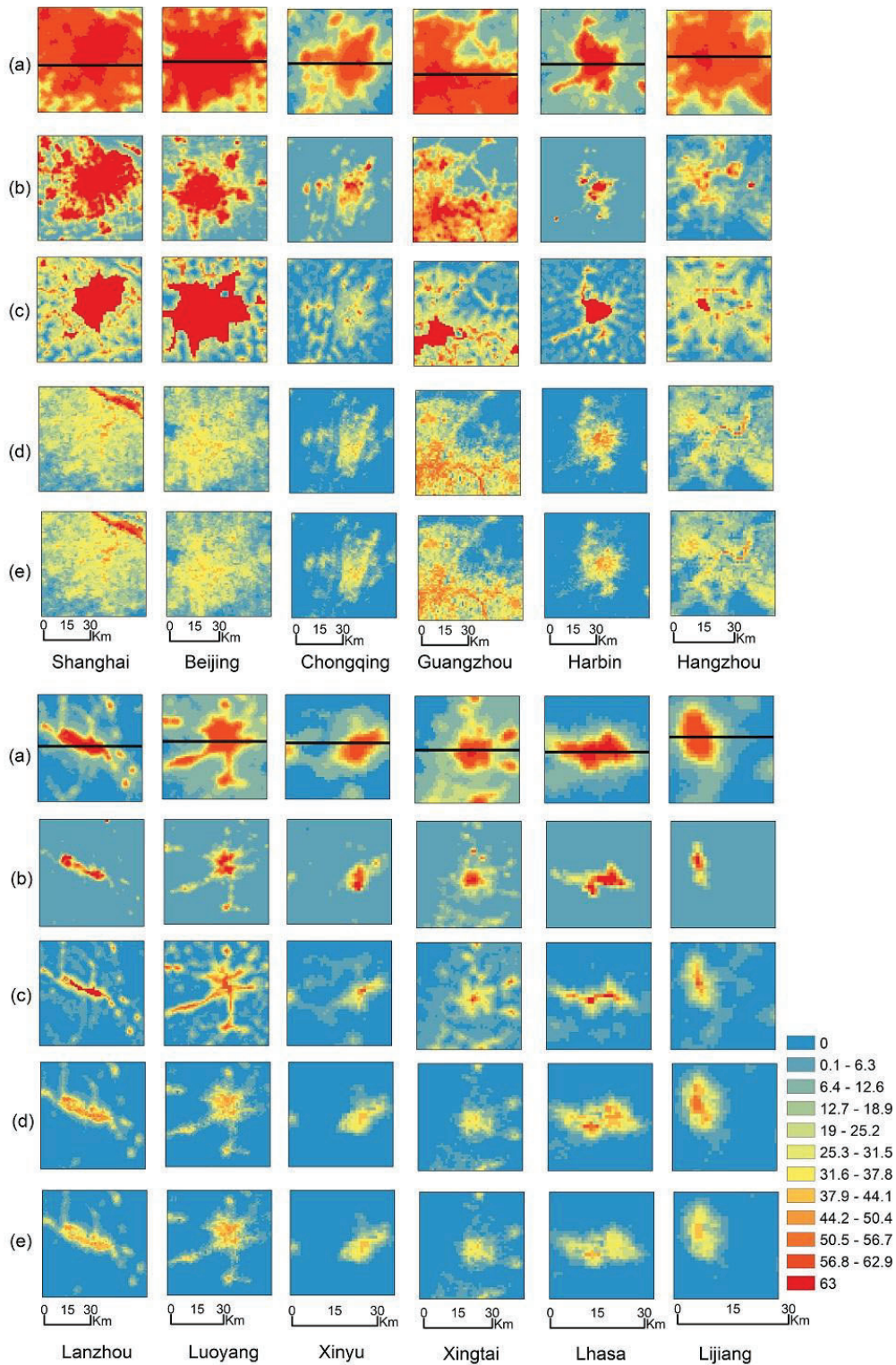
339

340 3.2 Visual evaluation

341 Fig. 4 shows the original DMSP images, the VIIRS images, the DMSP-BC images, and the
 342 VANUI and VTLI images of the twelve cities with populations from less than 0.5 million to over
 343 10 million. To make these images visually comparable, the NPP-VIIRS, VANUI and VTLI
 344 images were linearly stretched to the range of the DMSP data using the minimum and maximum
 345 pixel values. It can be observed from Fig. 4 that the DMSP data suffered from a strong blooming
 346 effect when compared with the VIIRS images, whereas the DMSP-BC images could shrink the
 347 boundaries of urban areas and decrease the values for urban outskirts. Compared with the DMSP
 348 images, the DMSP-BC, VANUI and VTLI images have higher spatial similarity with the VIIRS
 349 images. In large cities, such as Shanghai, Beijing, Guangzhou and Hangzhou, we can observe
 350 some line objects (e.g., roads) in the DMSP-BC or VIIRS images that are totally covered by the
 351 blooming effect in the original DMSP images. However, for Shanghai and Beijing in the VANUI
 352 and VTLI images, the urban centers have low DN values, which might result from the high
 353 vegetation coverage in these regions. In Chongqing, Harbin, Lanzhou, Luoyang, Xinyu, Xingtai,
 354 Lhasa and Lijiang, dark pixels in the VIIRS images (the rural areas) were brightened in the

355 original DMSP images due to the effect of blooming, whereas these pixels are adjusted to nearly
356 zero in the DMSP-BC images. Visual inspection of these twelve cities indicate that the SEAM
357 model can mitigate the blooming effect of the original DMSP image.

358

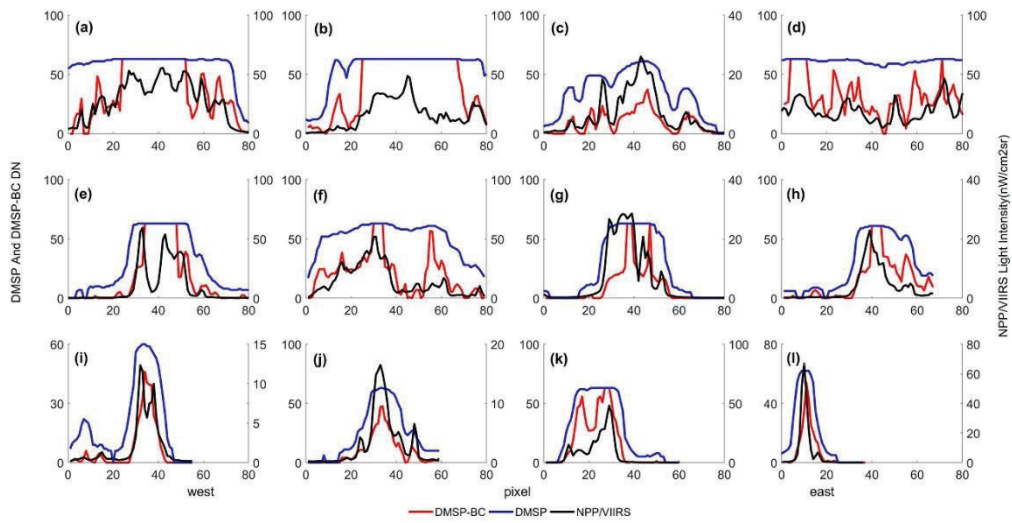


359

360 Fig. 4. Comparison of the NTL images in the twelve cities of China: (a) the original DMSP-OLS
 361 images, (b) the NPP-VIIRS images, (c) the DMSP-BC images, (d) the VANUI images, and (e)
 362 the VTLI images. The black lines are transects whose values are plotted in Fig. 5.

363
364
365
366
367
368
369
370
371
372
373
374
375
376
377
378
379
380

Fig. 5 shows the DN values of the transects in the DMSP images (blue lines), VIIRS images (black lines) and DMSP-BC images (red lines) for the twelve cities. It can be observed that all three NTL images have lower DN values in rural areas and higher values in urban areas, especially in the city center. The values of the DMSP-BC images are smaller than those of the original DMSP images after removing the blooming parts, especially in the rural regions. These transects also show that the variations of DN values in the DMSP-BC images have greater similarity with the VIIRS images compared with the DMSP images. Moreover, the variation of DN values in the urban areas of the DMSP images is smaller than those of the DMSP-BC and VIIRS images. For transects of Shanghai, Beijing and Guangzhou (Fig. 5 a, b and d), many saturated values in the DMSP images close to urban cores were also adjusted into lower values in the DMSP-BC images. This result suggests that the SEAM model can also partly remove the effect of saturation. In the rural areas where DN values of VIIRS are close to zero, the DMSP images maintain high values of approximately 10–20 (e.g., the west part of Lanzhou, Luoyang and Xinyu in Fig. 5 g, h and i) due to the blooming effect, and the DN values of these pixels in the DMSP-BC image were adjusted to 0–5. These transects suggest that the SEAM model can effectively remove the blooming effect and partly remove the saturation effect in DMSP images.



381

382 Fig. 5. Profiles of transects (the black lines in Fig. 4) of Shanghai (a), Beijing (b), Chongqing (c),
 383 Guangzhou (d), Harbin (e), Hangzhou (f), Lanzhou (g), Luoyang (h), Xinyu (i), Xingtai (j),
 384 Lhasa (k), and Lijiang (l) from the DMSP, VIIRS and DMSP-BC images.

385

386 3.3 Quantitative evaluation

387 Table 1 lists the correlation coefficients (R) with VIIRS images for DMSP, DMSP-BC,
 388 VANUI and VTLI and CV values calculated by Eq. (8) for DMSP, VIIRS, DMSP-BC, VANUI
 389 and VTLI in twelve selected cities and the whole of China, excluding pixels with DN equal to 0
 390 in the DMSP-BC image. When comparing original DMSP and DMSP-BC images, the
 391 correlation coefficients with VIIRS images in the whole of China are 0.62 and 0.69 for the
 392 original DMSP and DMSP-BC images, respectively, whereas all twelve cities have higher
 393 correlation coefficients after blooming effect correction by the SEAM model. The increase of the
 394 correlation coefficients indicates that the DMSP-BC images are more similar to the VIIRS
 395 images compared with the original DMSP images. In terms of spatial variability, the images after
 396 blooming effect removal for all twelve cities can have higher CVs than the original DMSP
 397 images. The CV values of the twelve cities from DMSP-BC are between the CV values from the
 398 DMSP and VIIRS images, and the CVs of the whole of China are 1.53, 0.94 and 2.64 for DMSP-

399 BC, DMSP, and VIIRS images, respectively, which suggests that the spatial variability of the
400 DMSP images was enhanced after blooming effect correction. However, the spatial variability of
401 the DMSP-BC images is still not as high as that of the VIIRS images. The possible reasons
402 include the existence of saturated pixels, the discrepancy of spatial resolutions between DMSP
403 and VIIRS, and the remaining blooming effect.

404 The results in Table 1 show that in some cities the DMSP-BC images from SEAM perform
405 better than VANUI and VTLI. The correlation results show lower values for VANUI and VTLI
406 in Shanghai, Beijing, Guangzhou, Hangzhou, Lhasa and Lijiang. The possible reason for this
407 result may be that the high percentage of green space makes the assumption of the two indexes
408 invalid. For the other cities, SEAM's results are comparable with those of VANUI and VTLI.
409 These results suggest that the auxiliary data, such as NDVI and LST, may introduce extra errors
410 in blooming correction. The CV values indicate similar spatial variabilities for SEAM, VANUI
411 and VTLI. We noticed that VANUI and VTLI show comparable or even better results than
412 SEAM in some cities; however, the auxiliary datasets required by these methods impede their
413 applicability.

414

415

416

417

418

Table 1 The quantitative evaluation of the DMSP, DMSP-BC, VANUI and VTLI images for the twelve cities and all of China

City/Province	Population* (million)	Correlation with VIIRS (R)			Spatial variability (CV)					
		DMSP	DMSP-BC	VANUI	VTLI	DMSP	VIIRS	DMSP-BC	VANUI	VTLI
Shanghai/Shanghai	13.64	0.643	0.769	0.648	0.661	0.409	1.080	0.797	0.535	0.523
Beijing/Beijing	12.45	0.629	0.784	0.751	0.760	0.533	1.594	1.103	0.932	0.948
Chongqing/Chongqing	8.52	0.785	0.801	0.841	0.845	0.676	1.090	1.021	1.376	1.394
Guangzhou/Guangdong	6.87	0.687	0.746	0.694	0.691	0.690	1.601	1.075	1.098	1.139
Harbin/Heilongjiang	4.74	0.612	0.768	0.775	0.781	0.917	3.128	1.721	2.084	2.111
Hangzhou/Zhejiang	4.51	0.636	0.698	0.605	0.615	0.332	1.070	0.705	0.720	0.724
Lanzhou/Gansu	2.47	0.702	0.747	0.772	0.780	0.951	2.453	1.590	1.214	1.246
Luoyang/Henan	1.93	0.771	0.797	0.877	0.882	0.786	1.652	1.311	1.327	1.352
Xinyu/Jiangxi	0.89	0.731	0.744	0.820	0.824	0.787	1.681	1.305	1.376	1.392
Xingtai/Hebei	0.87	0.725	0.738	0.811	0.815	0.717	1.527	1.205	1.176	1.193
Lhasa/Xizang	0.30	0.680	0.685	0.649	0.662	0.796	1.904	1.314	1.098	1.122
Lijiang/Yunnan	0.15	0.706	0.877	0.808	0.770	0.920	2.287	1.470	1.228	1.184
Whole China	/	0.619	0.694	0.702	0.711	0.936	2.639	1.530	1.538	1.574

* The populations of each city in 2013 were collected from the China City Statistical Yearbook 2014 (National Bureau of Statistics of China, 2014).

423 **3.4 Urban area extraction**

424 The results of urban areas extraction are shown in Fig. 6 and Table 2. Fig. 6 indicates that
 425 the spatial distributions of the urban areas are more similar to the GUF data after blooming effect
 426 removal. For example, the urban region of Shanghai extracted from the DMSP data by the local
 427 optimal threshold is only the urban core area, whereas the DMSP-BC result could extract the tiny
 428 urban regions that also exist in the GUF image. Table 2 lists the urban areas of the 12 cities
 429 extracted from the DMSP and DMSP-BC images as well as the reference urban areas from the
 430 GUF data. Table 2 also shows differences in urban areas between GUF and DMSP (denoted as
 431 Difference_DMSP) and between GUF and DMSP-BC (denoted as Difference_DMSP-BC). From
 432 Table 2 we find that the areas of the urban areas extracted from the DMSP-BC images are closer
 433 to the reference values than those from the DMSP data. The kappa coefficients in Table 2 also
 434 confirm that urban areas extracted from DMSP-BC are more similar to the GUF reference than
 435 those from DMSP. In conclusion, DMSP images after removing the blooming effect by the
 436 SEAM model can obtain more accurate urban extents than the original DMSP data.

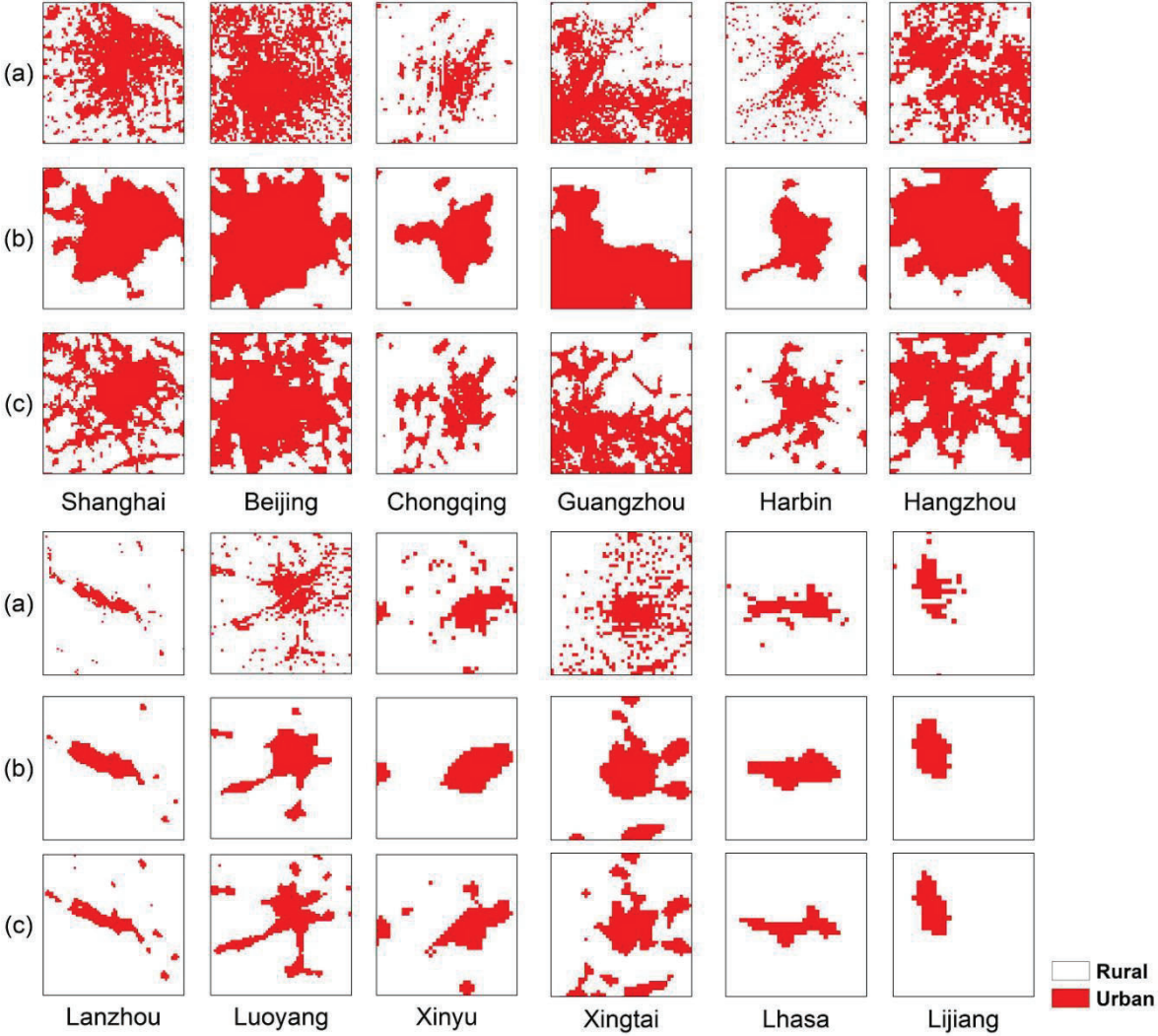
437

438 Table 2 Urban areas extracted from the DMSP and DMSP-BC images for the twelve cities
 439 (unit=km²)

City/Province	Kappa for DMSP	Kappa for DMSP-BC	Area from DMSP	Area from DMSP-BC	Area from GUF	Difference_DMSP	Difference_DMSP-BC
Shanghai/Shanghai	0.7302	0.7382	2399	2798	2798	399	0
Beijing/Beijing	0.7756	0.8437	3754	4294	4359	605	65
Chongqing/Chongqing	0.5181	0.6604	1058	992	711	347	281
Guangzhou/Guangdong	0.7364	0.7950	11274	10962	9221	2053	1741
Harbin/Heilongjiang	0.6718	0.8120	975	1153	1266	291	113
Hangzhou/Zhejiang	0.6200	0.6317	2005	1908	1712	293	196
Lanzhou/Gansu	0.5925	0.7823	359	320	330	29	10
Luoyang/Henan	0.6652	0.8639	518	596	672	154	76
Xinyu/Jiangxi	0.6401	0.7305	177	205	209	32	4
Xingtai/Hebei	0.4713	0.6916	500	495	576	76	81

Lhasa/Xizang	0.3767	0.4581	120	86	99	21	13
Lijiang/Yunnan	0.7160	0.8843	65	56	59	6	3

440
441



442

443 Fig. 6. Comparison of the urban area of (a) the Global Urban Footprint images at 1-km resolution
444 (GUF-1km) and urban area extracted from (b) DMSP-OLS images and (c) DMSP-BC images in
445 the twelve cities of China

446

447 **4. Discussion and Conclusions**

448 DMSP datasets are useful for studying regional economic development because of their
449 strong relationship with economic development, energy consumption and population. However,

450 DMSP datasets severely suffer from saturation and blooming effects. This research proposed a
451 simple blooming effect correction method, the self-adjusting model (SEAM), based on spatial
452 response functions without using any ancillary data. The SEAM model was tested in the whole
453 of China and produced blooming-effect-corrected images, e.g., DMSP-BC, compared with the
454 original DMSP and NPP-VIIRS images. The visual and quantitative evaluations as well as the
455 results of urban area extraction suggested that the SEAM model can largely remove the
456 blooming effect in the original DMSP dataset and enhance its spatial quality.

457 The greatest strength of the SEAM method is that it estimates the important parameters in
458 the spatial spread function from the DMSP image itself rather than requiring any other ancillary
459 data, and the estimated parameters are then used to remove blooming effects on all DMSP pixels.
460 This advantage makes the SEAM method very applicable and easy to implement. In contrast,
461 existing methods, such as the frequency threshold method ([Small et al., 2005](#)) and the overflow
462 removal model ([Townsend and Bruce, 2010](#)), need other ancillary datasets and extra effort. The
463 frequency threshold method ([Small et al., 2005](#)) needs urban extent derived from Landsat images
464 to determine the optimal frequency threshold, and this study also suggested that it is very
465 difficult to find one threshold that works for a majority of cities in the world. The overflow
466 removal model is an iterative process that needs administrative division boundaries as masks and
467 census population data to stop the iterative process ([Townsend and Bruce, 2010](#)); moreover, this
468 model was only tested in Australia due to the availability of an ancillary dataset.

469 The second strength of the SEAM method is that the SEAM model was developed based
470 on reasonable assumptions, one of which is that DMSP images have pseudo light pixels (PLPs),
471 i.e., pixels containing little artificial light source but lit by neighboring light sources. The pixels
472 adjacent to the background were defined as PLPs, and their neighbors with larger DN values

473 were used as neighboring light sources. Such PLPs should exist in any countries that have cities
474 visible in the DMSP images. Another assumption is that the effective blooming distance is
475 approximately 3.5 km, and a 7×7 moving window was thus used to removing blooming from the
476 neighboring pixels. We investigated the effective blooming distance in 20 isolated cities using a
477 land cover product, GlobeLand30 (Chen et al., 2015; Chen et al., 2016). Table 3 lists the
478 effective blooming distances and the average light intensities measured from the DMSP image,
479 mean concentrations of PM_{2.5} at ground-level (van Donkelaar et al., 2016) and neighboring water
480 areas of the 20 cities. The results indicate that the smallest distance is 2.22 km in Turpan (No. 04
481 in Fig. 1a) and the largest is 4.38 km in Jinchang (No. 08 in Fig. 1a). The average distance for 20
482 cities is 3.53 km, which is equivalent to 3.5 pixels in DMSP images. Therefore, it is reasonable
483 to use the 7×7 window to define the neighboring pixels whose blooming light can reach the pixel
484 at the window center. We also found that this effective blooming distance is not related to the
485 average light intensity of the city ($R=0$, $p=0.50$) and PM_{2.5} concentration ($R=0.10$, $p=0.35$),
486 which suggests that the 7×7 window is good for cities with different sizes and under different
487 atmospheric conditions. An experiment using different window sizes suggests that the proposed
488 method is not very sensitive to the window size (see Supplementary Data). Therefore, the 7×7
489 window should obtain acceptable accuracy and is recommended for most areas, although we
490 suggest further studies to test the parameter in more countries. Note that the effective blooming
491 distance may be longer than 3.5 km in coastal cities or cities with many water surfaces. From the
492 20 cities listed in Table 3, the effective blooming distance is positively correlated to the water
493 area surrounding a city ($R=0.53$, $p<0.05$). Although the 7×7 window can obtain satisfactory
494 results of blooming effect removal by the SEAM model for coastal cities (see Supplementary
495 Data), a larger window is recommended for processing DMSP images in coastal areas.

Table 3 Effective blooming distance for 20 cities in China

Serial number	City/Province	Effective blooming distance (km)	Average light intensity of the city (DN)	PM _{2.5} concentration (µg/m ³)	Water area surrounding the city (km ²)*
01	Xilinhot/Inner Mongolia	4.08	15.37	16.77	1.24
02	Hami/Xinjiang	3.31	23.13	18.30	0.21
03	Korla/Xinjiang	2.49	13.93	17.80	0.46
04	Turpan/Xinjiang	2.22	14.70	16.39	0.00
05	Jiuquan/Gansu	2.84	14.14	29.10	0.35
06	Bayannur/Inner Mongolia	2.36	23.10	23.79	0.00
07	Xinzhou/Shanxi	3.27	19.15	31.61	0.00
08	Jinchang/Gansu	4.38	16.60	36.35	1.18
09	Yan'an/Shaanxi	2.73	10.65	38.20	1.42
10	Yushu/Qinghai	3.36	13.38	31.12	1.00
11	Delingha/Qinghai	3.63	13.40	43.73	0.84
12	Tianshui/Gansu	4.39	14.92	6.65	3.89
13	Xuancheng/Anhui	3.31	12.36	64.36	0.22
14	Lhasa/Xizang	4.35	18.54	29.64	9.99
15	Enshi/Hubei	3.07	16.61	27.83	0.18
16	Jiujiang/Jiangxi	3.74	19.66	29.19	3.45
17	Chongqing/Chongqing	4.32	14.29	29.35	0.59
18	Huaihua/Hunan	4.33	17.16	39.42	10.56
19	Ji'an/Jiangxi	4.01	14.72	31.50	0.21
20	Kaili/Guizhou	4.33	15.40	32.26	2.11
Average		3.53	16.06	29.67	1.89

498 *The water area surrounding each city was calculated by the range of effective blooming distance for each city.

499 Both the urban extent and water surface were provided by the GlobeLand30-2010 land cover product.

500

501 The third strength is that the proposed SEAM method optimizes the parameters in the
 502 adjustment model locally rather than globally. Blooming effect intensity, represented by the
 503 regression coefficient a (Fig. 3b), was found to be positively correlated with the annual mean
 504 PM_{2.5} concentration ($R^2 = 0.3223$, $p < 0.0001$), which suggests that the blooming effect is
 505 strengthened by the scattering of aerosol particles in the air (Xu et al., 2015). Considering that
 506 the PM_{2.5} concentration varies in space, it is necessary to build the adjusting model for removing
 507 the blooming effect in DMSP images locally.

508 In this study, we only tested the SEAM model in China, and more countries should be used
 509 to further evaluate the effectiveness of our method. We did not compare the SEAM model with
 510 many other methods, such as the ORM model (Townsend and Bruce, 2010) because it is difficult

511 to collect the auxiliary data required by these methods. Some saturation pixels remained in the
512 blooming-effect-corrected images for big cities, e.g., Shanghai, Beijing, Guangzhou and Harbin
513 (Fig. 4). Saturation correction methods (Zhang et al., 2013; Zhuo et al., 2015; Hao et al., 2015)
514 could further improve the quality of DMSP data after applying the proposed method. By
515 mitigating the blooming effect in DMSP images by the proposed SEAM method, the corrected
516 DMSP images are expected to map the socioeconomic parameters and monitor urbanization
517 processes with improved performance (see an example in the Supplementary Data). Note that
518 blooming correction is not necessary for other applications such as mapping light pollution. Due
519 to its simple principle, the SEAM method has the potential to produce blooming-adjusted DMSP
520 NTL images in large areas. The SEAM model requires computational resources to select PLPs
521 and build regression models for each pixel. Processing the entire region of China (5074×4001
522 pixels) required approximately 17 hours using one CPU of a quad-core desktop computer (3.3
523 GHz, Intel(R) Core(TM) i5-4590). The computational efficiency can be further improved by
524 parallel computing and high-performance computers.

525

526 **Acknowledgements**

527 This study was supported by the Taishan Scholar Program of Shandong Province, China, the
528 Research Grants Council of Hong Kong (No. 25222717), the National Natural Science
529 Foundation of China (Nos. 41701627 and 41701378), the Fund for Creative Research Groups of
530 the National Natural Science Foundation of China (41621061), and a research grant from The
531 Hong Kong Polytechnic University (No. 1-ZE6Q).

532

533 References

- 534 Abrahams A, Oram C, Lozano-Gracia N. Deblurring DMSP nighttime lights: A new method
535 using Gaussian filters and frequencies of illumination[J]. *Remote Sensing of Environment*,
536 2018, 210: 242-258.
- 537 Bennett, M.M., Smith, L.C., 2017. Advances in using multitemporal night-time lights satellite
538 imagery to detect, estimate, and monitor socioeconomic dynamics. *Remote Sens. Environ.*
539 192, 176–197.
- 540 Butt, M.J., 2012. Estimation of Light Pollution Using Satellite Remote Sensing and Geographic
541 Information System Techniques. *GISci. Remote Sens.* 49, 609–621.
- 542 Cao, X., Chen, J., Imura, H., Higashi, O., 2009. A SVM-based method to extract urban areas
543 from DMSP-OLS and SPOT VGT data. *Remote Sens. Environ.* 113, 2205–2209.
- 544 Cao, X., Wang, J., Chen, J., Shi, F., 2014. Spatialization of electricity consumption of China
545 using saturation-corrected DMSP-OLS data. *Int. J. Appl. Earth Obs. Geoinf.* 28, 193–200.
- 546 Chen, J., Chen, J., Liao, A., Cao, X., Chen, L., Chen, X., He, C., Han, G., Peng, S., Lu, M.,
547 Zhang, W., Tong, X., Mills, J., 2015. Global land cover mapping at 30 m resolution: A
548 POK-based operational approach. *ISPRS-J. Photogramm. Remote Sens.* 103, 7–27.
- 549 Chen, X., Cao, X., Liao, A., Chen, L., Peng, S., Lu, M., Chen, J., Zhang, W., Zhang, H., Han, G.,
550 Wu, H., Li, R., 2016. Global mapping of artificial surfaces at 30-m resolution. *Sci. China-*
551 *Earth Sci.* 59(12), 2295–2306. DOI: 10.1007/s11430-016-5291-y.
- 552 Cinzano, P., Falchi, F., Elvidge, C. D., 2001. The first world atlas of the artificial night sky
553 brightness. *Mon. Not. Roy. Astron. Soc.* 328(3), 689–707.
- 554 Elvidge, C.D., Baugh, K.E., Kihn, E.A., Kroehl, H.W., Davis, E.R., Davis, C.W., 1997a.
555 Relation between satellite observed visible-near infrared emissions, population, economic
556 activity and electric power consumption. *Int. J. Remote Sens.* 18(6), 1373–1379.
- 557 Elvidge, C.D., Baugh, K.E., Kihn, E.A., Kroehl, H.W., Davis, E.R., 1997b. Mapping city lights
558 with nighttime data from the DMSP operational linescan system. *Photogramm. Eng.*
559 *Remote. Sens.* 63, 727–734.
- 560 Elvidge, C.D., Imhoff, M.L., Baugh, K.E., Hobson, V.R., Nelson, I., Safran, J., Tuttle, B.T.,
561 2001. Night-time lights of the world: 1994-1995. *ISPRS-J. Photogramm. Remote Sens.*
562 56(2), 81-99.
- 563 Elvidge, C.D., Jeffrey Safran, I. Nelson, B. Tuttle, V. Ruth Hobson, Kimberly E. Baugh, John B.
564 Dietz, Edward H. Erwin, R. Lunetta, and J. Lyon. *Area and positional accuracy of DMSP*
565 *nighttime lights data*. CRC Press: Boca Raton, FL, USA, 2004.
- 566 Elvidge, C.D., Cinzano, P., Pettit, D.R., Arvesen, J., Sutton, P., Small, C., Nemani, R., Longcore,
567 T., Rich, C., Safran, J., Weeks, J., Ebener, S., 2007. The Nightsat mission concept. *Int. J.*
568 *Remote Sens.* 28(12), 2645–2670.
- 569 Elvidge, C.D., Ziskin, D., Baugh, K.E., Tuttle, B.T., Ghosh, T., Pack, D.W., Erwin, E.H.,
570 Zhizhin, M., 2009. A fifteen year record of global natural gas flaring derived from satellite
571 data. *Energies* 2, 595–622.
- 572 Elvidge, C.D., Baugh, K., Zhizhin, M., Hsu, F -C. (2013). Why VIIRS data are superior to
573 DMSP for mapping nighttime lights? *Proceedings of the 35th meeting of the Asia Pacific*
574 *Advanced Network* 2013 35, 62-69.
- 575 Elvidge, C. D., Baugh, K. E., Zhizhin, M., Hsu, F -C., Ghosh, T., 2017. VIIRS night-time lights.
576 *Int. J. Remote Sens.* 38(21), 5860–5879.

577 Esch, T., Heldens, W., Hirner, A., Keil, M., Marconcini, M., Roth, A., Zeidler, J., Dech, S.,
578 Strano, E., 2017. Breaking new ground in mapping human settlements from space-The
579 Global Urban Footprint. *ISPRS-J. Photogramm. Remote Sens.* 134, 30–42.

580 Falchi, F., Cinzano, P., Duriscoe, D., Kyba, C.C.M., Elvidge, C.D., Baugh, K., Portnov, B.A.,
581 Rybnikova, N.A., Furgoni, R., 2016. The new world atlas of artificial night sky brightness.
582 *Sci. Adv.* 2, no. 6: e1600377.

583 Hao, R., Yu, D., Sun, Y., Cao, Q., Liu, Y., Liu, Y., 2015. Integrating multiple source data to
584 enhance variation and weaken the blooming effect of DMSP-OLS light. *Remote Sens.* 7,
585 1422–1440, doi:10.3390/rs70201422.

586 Hu, J., Wang, Y., Ying, Q., Zhang, H., 2014. Spatial and temporal variability of PM2.5 and
587 PM10 over the North China Plain and the Yangtze River Delta, China. *Atmos. Environ.* 95,
588 598–607.

589 Henderson, J.V., Storeygard, A., Weil, D.N., 2012. Measuring economic growth from outer
590 space. *Am. Econ. Rev.* 102, 994–1028. <http://dx.doi.org/10.1257/aer.102.2.994>.

591 Imhoff, M.L., Lawrence, W.T., Stutzer, D.C., Elvidge, C.D., 1997. A technique for using
592 composite DMSP/OLS “city lights” satellite data to map urban area. *Remote Sens.*
593 *Environ.* 61:361–370. [http://dx.doi.org/10.1016/S0034-4257\(97\)00046-1](http://dx.doi.org/10.1016/S0034-4257(97)00046-1).

594 Kyba, C., Garz, S., Kuechly, H., de Miguel, A.S., Zamorano, J., Fischer, J., Hölker, F., 2014.
595 High-resolution imagery of earth at night: new sources, opportunities and challenges.
596 *Remote Sens.* 7(1), 1-23.

597 Letu, H., Hara, M., Tana, G., Bao, Y., Nihio, F., 2015. Generating the nighttime light of the
598 human settlements by identifying periodic components from DMSP/OLS satellite imagery.
599 *Environ. Sci. Technol.* 49, 10503–10509.

600 Letu, H., Hara, M., Yagi, H., Naoki, K., Tana, G., Nishio, F., Shuhe, O., 2010. Estimating
601 energy consumption from night-time DMSP/OLS imagery after correcting for saturation
602 effects. *Int. J. Remote Sens.* 31, 4434–4458.

603 Levin, N., 2017. The impact of seasonal changes on observed nighttime brightness from 2014 to
604 2015 monthly VIIRS DNB composites. *Remote Sens. Environ.* 193, 150–164.

605 Li, X., Li, D., Xu, H., Wu, C., 2017. Intercalibration between DMSP/OLS and VIIRS night-time
606 light images to evaluate city light dynamics of Syria’s major human settlement during
607 Syrian Civil War. *Int. J. Remote Sens.* 38, 5934–5951. Li, X., Zhou, Y., 2017. Urban
608 mapping using DMSP/OLS stable night-time light: a review. *Int. J. Remote Sens.* 38,
609 6030–6046. doi:10.1080/01431161.2016.1274451.

610 Liang, S., 2003. *Quantitative Remote Sensing of Land Surfaces*. John Wiley & Sons, Inc., New
611 Jersey.

612 Lo, C.P., 2002. Urban indicators of China from DN-calibrated digital DMSP-OLS nighttime
613 images. *Ann. Assoc. Am. Geogr.* 92, 225–240.

614 Longcore, T., Rich, C., 2004. Ecological light pollution. *Front. Ecol. Environ.* 2, 191-198.

615 Lu, D., Tian, H., Zhou, G., Ge, H., 2008. Regional mapping of human settlements in
616 southeastern China with multisensor remotely sensed data. *Remote Sens. Environ.* 112,
617 3668–3679.

618 National Bureau of Statistics of China. *China city statistical yearbook 2014*. China Statistics
619 Press, Beijing, 2014.

620 Pandey, B., Zhang, Q., Seto, K. 2017. Comparative evaluation of relative calibration methods for
621 DMSP/OLS nighttime lights. *Remote Sens. Environ.* 195, 67–78.

622 Proville, J., Zavala-Araiza, D., Wagner, G., 2017. Night-time lights: A global, long term look at
623 links to socio-economic trends. *PLoS One* 12(3): e0174610.
624 <https://doi.org/10.1371/journal.pone.0174610>

625 Richter, R., 1996. A spatially adaptive fast atmospheric correction algorithm. *Int. J. Remote Sens.*
626 17(6), 1201–1214.

627 Rodrigues, P., Aubrecht, C., Gil, A., Longcore T., Elvidge, C., 2012. Remote sensing to map
628 influence of light pollution on Cory's shearwater in Sao Miguel Island, Azores
629 Archipelago. *Eur. J. Wildl. Res.* 58, 147–155.

630 Rohner, D., Thoenig, M., Zilibotti, F., 2013. Seeds of distrust: conflict in Uganda. *J. Econ.*
631 *Growth* 18:217–252. <http://dx.doi.org/10.1007/s10887-013-9093-1>.

632 Small, C., Elvidge, C.D., Balk, D., Montgomery, M., 2011. Spatial scaling of stable night lights.
633 *Remote Sens. Environ.* 115, 269–280. <http://dx.doi.org/10.1016/j.rse.2010.08.021>.

634 Small, C., Elvidge, C.D., 2013. Night on Earth: Mapping decadal changes of anthropogenic night
635 light in Asia. *Int. J. Appl. Earth Obs. Geoinf.* 22, 40–52.

636 Small, C., Pozzi, F., Elvidge, C.D. 2005. Spatial analysis of global urban extent from DMSP-
637 OLS night lights. *Remote Sens. Environ.* 96, 277–291.

638 Townsend, A.C., Bruce, D.A., 2010. The use of night-time lights satellite imagery as a measure
639 of Australia's regional electricity consumption and population distribution. *Int. J. Remote*
640 *Sens.* 31(16), 4459–4480.

641 van Donkelaar, A., Martin, R.V., Brauer, M., Hsu, N.C., Kahn, R.A., Levy, R.C, Lyapustin, A.,
642 Sayer, A.M., Winker, D. M., 2016. Global Estimates of Fine Particulate Matter using a
643 Combined Geophysical-Statistical Method with Information from Satellites, Models, and
644 Monitors. *Environ. Sci. Technol.* 50, 3762–3772, doi: 10.1021/acs.est.5b05833.

645 Wang, J., Aegerter, C., Xu, X., Szykman, J.J., 2016. Potential application of VIIRS Day/Night
646 Band for monitoring nighttime surface PM_{2.5} air quality from space. *Atmos. Environ.* 124,
647 55–63.

648 Xie, Y., Weng, Q., 2017. Spatiotemporally enhancing time-series DMSP/OLS nighttime light
649 imagery for assessing large-scale urban dynamics. *ISPRS-J. Photogramm. Remote Sens.*
650 128, 1–15.

651 Xu, Z., Xia, X., Liu, X., Qian, Z., 2015. Combining DMSP/OLS nighttime light with echo state
652 network for prediction of daily PM_{2.5} average concentrations in Shanghai, China.
653 *Atmosphere* 6, 1507–1520, doi:10.3390/atmos6101507.

654 Zhang, Q., Schaaf, C., Seto, K. C., 2013. The vegetation adjusted NTL urban index: A new
655 approach to reduce saturation and increase variation in nighttime luminosity. *Remote Sens.*
656 *Environ.* 129, 32–41. doi:10.1016/j.rse.2012.10.022.

657 Zhang, X., Wu, J., Peng, J., Cao, Q., 2017. The Uncertainty of Nighttime Light Data in
658 Estimating Carbon Dioxide Emissions in China: A Comparison between DMSP-OLS and
659 NPP-VIIRS. *Remote Sens.* 9(8), 797; doi:10.3390/rs9080797.

660 Zhou, Y., Smith, S. J., Elvidge, C. D., Zhao, K., Thomson, A., Imhoff, M., 2014. A cluster-based
661 method to map urban area from DMSP/OLS nightlights. *Remote Sens. Environ.* 147, 173–
662 185.

663 Zhou, Y., Smith, S.J., Zhao, K., Imhoff, M., Thomson, A., Bond-Lamberty, B., Asrar, G.R.,
664 Zhang, X., He, C., Elvidge, C.D., 2015. A global map of urban extent from nightlights.
665 *Environ. Res. Lett.* 10. doi:10.1088/1748-9326/10/5/054011.

666 Zhuo, L., Ichinose, T., Zheng, J., Chen, J., Shi, P.J., Li, X., 2009. Modeling the population
667 density of China at the pixel level based on DMSP/OLS non-radiance calibrated nighttime
668 light image. *Int. J. Remote Sens.* 30 (4), 1003–1018.
669 Zhuo, L., Zheng, J., Zhang, Z., Li, J., Liu, L. 2015. An improved method of night-time light
670 saturation reduction based on EVI. *Int. J. Remote Sens.* 36 (16), 4114–4130,
671 <http://dx.doi.org/10.1080/01431161.2015.1073861>.
672